

Abstract

The deposition of fluvial sediments in tectonically active areas is mainly controlled by tectonics, climate, and associated Earth surface processes; consequently, fluvial sediments can provide a valuable record of changes in regional climate and tectonic activity. In this study, we conducted a detailed analysis of the grain-size distribution in modern fluvial sediments from the upper Min River, Eastern Tibet. These data, combined with information of regional climate, vegetation, hydrology, geomorphology, lithology, and fault slip rate, indicate that modern regional tectonic activity along upper Min River can be divided into three segments. Specifically, fluvial sediments in Minjiangyuan - Diexi segment~~the segment I~~ are dominated by silts ($<63\text{ }\mu\text{m}$, 70.2%), agreeing with a low-runoff, low-rainfall and high vegetation cover and revealing a windblown origin influenced by the arid and windy climate. These observations are consistent with the low hillslope angle and low relief~~in segment I~~, all indicating weak activity along the Minjiang Fault. The coarse-grained fraction ($>250\text{ }\mu\text{m}$) of fluvial sediments in Diexi - Wenchuan and Wenchuan - Dujiangyan segments~~the segments II and III~~ increases stepwise downstream, although runoff and rainfall do not change significantly~~from segment II to segment III~~. These patterns correlate well with increases in both regional relief and hillslope angles. Together, these observations imply that regional tectonic activity along Maoxian-Wenchuan Fault becomes more pervasive downstream along the Min River. The occurrence of well-sorted and well-rounded pebbles of fluvial sediments in downstream of Dujiangyan must be related to the long-time scouring and sorting by rivers. This study marks the first development of

36 a new ~~and important~~ research approach that can characterize regional tectonic activity
37 by analysis of grain-size distribution of fluvial sediments collected from tectonically
38 active regions.

39

40 **Keywords:** Modern fluvial sediments; Grain-size analysis; Tectonic activity; Upper
41 Min River; Eastern Tibetan Plateau

42

1 Introduction

Tectonic geomorphology is a relatively young sub-discipline of geomorphology, and has the major aim of unraveling interactions between tectonic activity, climate, and Earth surface processes (Wobus et al., 2005; Owen, 2013). The grain-size distribution of river bed material, channel width, channel sinuosity, extent of alluvial cover, lithology of bedrock, and hydraulic roughness are all potentially important variables (Whipple, 2004; Whittaker et al., 2010). Although many factors determine the grain-size distribution of fluvial sediments, but there are one or two mainly controlling factors in specific regions. Previous studies have shown that it is feasible to discuss the main control factors for changes in grain-size of fluvial sediments (Singh et al., 2007; Bravard et al., 2014). ThusIn addition, comprehensive amounts of data must be collected in a wide range of field settings before the responses of these important variables to climatic and tectonic forcings can be determined.

The topographic margin of the Tibetan Plateau (TP) along the Longmen Shan is one of the most impressive continental escarpments in the world, and the land surface rises westward over a horizontal distance of 40–60 km from the Sichuan Basin (500–700 m elevation) to peak elevations exceeding 6000 m (Chen et al., 2000; Kirby et al., 2000, 2008). Some studies have revealed common topographic features within river channels in the eastern TP, namely, an upper low-gradient channel segment, a middle steep-gradient channel segment, and a low~~er-lying~~ very steep channel segment, such as in the Red River region in Yunnan Province (Schoenbohm et al., 2004) and the Min River region in Sichuan Province (Kirby et al., 2003). However, it is important to note that strong lithological contrasts along the ~~length-of-a~~ river can also cause the channel

steepness index to change at comparable magnitudes to those associated with large gradients in rock uplift rate (Snyder et al. 2000; [Beek and Bishop, 2003](#); Stock and Dietrich, 2003; ~~Beek and Bishop 2003~~; Whittaker et al., 2010). New data sourced from several localities record an apparent narrowing of channel width in response to increased rock uplift rates in rivers with large areas of bedrock (Whipple, 2004). This is consistent with the recent proposition that river profiles straighten as aridity increases (Chen et al., 2019), as observed along the upper Min River in the field. Generally, exposures of hard bedrock often generate straight channels, which have low channel slopes and small sediment loads (Schumm and Khan, 1971, 1972).

Vegetation density can modulate topographic responses to changing denudation rates, such that the functional relationship between denudation rate and topographic steepness becomes increasingly linear as vegetation density increases (Olen et al., 2016). Recent studies indicate that the upper Min River has poor vegetation coverage and most regions are fully exposed due to the strongly arid climate conditions (Jiang et al., 2015; [Shi et al., 2020](#); Xu et al., 2020; ~~Shi et al., 2020~~; Wei et al., 2021; Zhou et al., 2021). Thus, hillslope colluvium is the dominant sediment source to the upper Min River — especially in its middle and lower ~~segments-parts~~ (Zhang et al., 2021) — akin to those in drainage basins in many arid regions worldwide (Clapp et al., 2002).

Tectonic activity influences the evolution of lacustrine sedimentary sequences by affecting the provenance supply (Najman, 2006; Jiang et al., 2022). Frequent earthquakes on the TP, as recorded by widely distributed soft sediment deformation (Wang et al., 2011; Xu et al., 2015; Jiang et al., 2016; Zhong et al., 2019; Zhang et al., 2021), caused repeated landslides that also represent another major source of sediment into the upper Min River (Dai et al., 2011; Xu et al., 2012, 2013). These landslides

generated a large amount of dust storms that deposited ~~dust~~ in nearby lakes (Jiang et al., 2014, 2017) and exposed large quantities of fine-grained sediment that had accumulated on mountain slopes, which were subsequently transported by wind to ancient lakes, documenting these seismic events (Whittaker et al., 2010; Liang and Jiang, 2017; Shi et al., 2022). This sedimentological process was recently recognized at Huojizhai, Diexi Town, following the ~~historical earthquake at 1933~~ M_s 7.5 Diexi ~~earthquake in 1933~~ (Wei et al., 2021).

Changes in hydrology and sediment flux are commonly regarded as climate forcing (Wobus et al., 2010). The ~~extent of~~ alluvial cover is very limited throughout the upper Min River Basin, which is demonstrated by similarity of zircon U-Pb ages in lacustrine sediments and their nearby bedrock units (Zhong et al., 2017). As such, the influence of occasional flood events should be considered over a longer time scales (Snyder and Whipple, 2003), as aridity precludes rainfall or fluvial undercutting as ~~being the triggers~~ for such events.

The consistent climate coupled with systematic variations in lithology and rock uplift rate along the Min Mountains allow comparison of channels that experience different tectonic forcings (Duvall et al., 2004). Selective transport is the dominant downstream fining mechanism in this region, although rates of selective transport in sand-bed rivers are smaller than those in gravel-bed rivers (Frings, 2008).

Only a small volume of sediment collected from a river bed is needed to produce a transformative understanding of the rates at which landscapes change (Blanckenburg, 2005). Study of these materials can reveal relationships between generation, transport (Clapp et al., 2000, 2002), and mixing of sediment (Perg et al., 2003; Nichols et al., 2005), under the help of the key topographic and/or lithologic features (e.g., relief, slope angle, and substrate characteristics) (Riebe et al., 2000; Riebe et al., 2001; Matmon et

al., 2003a, b). The Min River is one of the important tributaries of the Yangtze River and goes through the climate transition zone and the tectonically active zone in the eastern TP. The alpine valleys along the Min River reduce the preservation potential of Quaternary sediments and expose large areas of bedrock, which hinder the study of tectonic activity. In this study, we combine field surveys and analysis of river sediments in the upper Min River to determine hydraulic characteristics, and topographic and tectonic information about bedrock channels.

2 Regional setting

2.1 Geographic and geologic settings

Instrumental data collected after 1900 indicate that the TP has experienced strong earthquakes clustered around the Bayan Kala Block from 1995 to the present ~~day~~, which are collectively known as the Kunlun—Wenchuan earthquake series (Deng et al., 2014). The eastern TP is ~~geomorphologically characterized by alpine valleys, and is~~ tectonically controlled by the Longmen Shan thrust belts, the Minjiang Fault, and the Huya Fault (Fig. 1a). Frequent tectonic activities have led to numerous earthquakes and landslides in this region (e.g., Zhang et al., 2003; Jiang et al., 2014; Li et al., 2015; Liang and Jiang, 2017), such as the 1933 Diexi M_s 7.5 earthquake, the 1976 Songpan M_s 7.2 earthquake, the 2008 Wenchuan M_s 8.0 earthquake and the 2017 Jiuzhaigou M_s 7.0 earthquake, which caused widespread geomorphic landscape damage, and released a large amount of fresh terrigenous debris. The sudden coarsening of grain-size in the Xinmocun and Lixian lacustrine sections is considered to be related to earthquakes (Jiang et al., 2014, 2017). ~~These earthquakes caused widespread damage to the Earth~~

~~surface in this region.~~ GPS-measured uplift rates in the Longmen Shan Fault zone reached 2–3 mm/a over 10 years since 1999 (Liang et al., 2013). Thermochronological dating of zircon and apatite indicated denudation rates of 1–2 mm/a in the Longmen Shan region during the Late Cenozoic (Kirby et al., 2002).

~~The alpine valleys in the eastern TP reduce the preservation potential of Quaternary sediments and expose large areas of bedrock.~~ Bedrock outcrops within the catchment region of the upper Min River are dominated by Silurian phyllite, quartz schist, and Triassic phyllite, metamorphosed sandstone (Fig. 1a), which are easily weathered and eroded into transportable debris (Zhong et al., 2019). Massive granites are also exposed in the study area; in particular, the Neoproterozoic Pengguan complex (U–Pb ages of 859–699 Ma; Ma et al., 1996) (Fig. 1a) is mainly composed of intermediate-acid intrusive rocks, with lesser amounts of basic-ultrabasic intrusive rocks, volcanic rocks, volcanoclastic rocks, and greenschist facies metamorphic rocks. Sand (> 63 μm) in the study area was recently demonstrated to have been mainly derived from local debris material, which itself is likely related to dust storms and loose surface material produced by seismic activity (Jiang et al., 2017; Liang and Jiang, 2017).

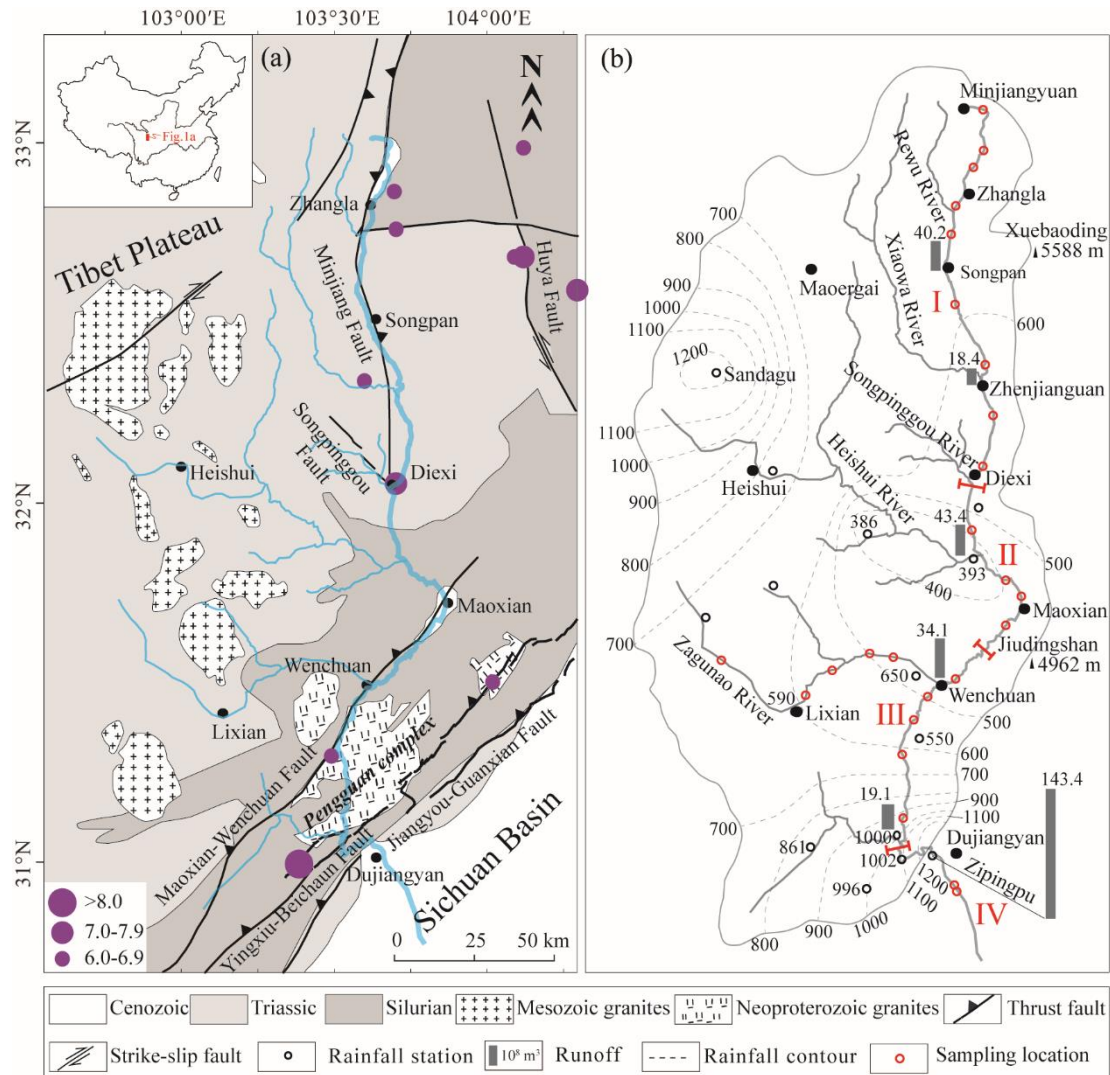


Figure 1 (a) Geological map and **(b)** precipitation distribution (Ding et al., 2014) for the upper Min River basin. Seismic data are from the China Earthquake Data Center (<http://data.earthquake.cn/data>).

The upstream channel of the Min River is ~340 km long (Li et al., 2005; Ding et al., 2014), nearly oriented N–S (Fig. 1b), and erodes the hinterland of the TP via formation of gullies and valleys. The Min River valley is typically steep, narrow and deepening downstream with an incision depth of 300–1500 m (e.g., Li et al., 2005; Zhang et al., 2005). The slopes on both sides of the study area ranges from are between

18° ~~to~~ ~~and~~ 45°, and the vertical aspect ratio of the valley ~~ranges from~~ ~~is~~ 5.5–12.6 %
(Zhang et al., 2005). Constrained by the specific landforms of the alpine valleys, the
wind direction in the study area is generally SSW/NNE, roughly consistent with the
strike of local valleys (Liu, 2014). The Min River valley exhibits high wind speeds in
April (~~average-mena~~ 4.9 m/s) and low speeds in July (~~average-mean~~ 3.7 m/s). Wind
speed is generally < 4 m/s before noon and > 4 m/s after noon, and normally peaks
approximately 8–10 m/s at around 16:00 (Liu, 2014). The highest instantaneous wind
speed recorded in the study area was 21 m/s (Liu, 2014).

The upper reaches of the Min River are located in a transition zone on the TP
where wet monsoonal climate changes to a high-elevation cold climate. In this region,
mean annual precipitation (MAP) ranges from 400 mm to 850 mm, and precipitation is
dominant (>75%) during the rainy season (~~May~~–October) (Ding et al., 2014). It is
noticeable that orographic rain along the eastern TP generates two storm areas centered
around Sandagu and Zipingpu (Fig. 1b). Statistical analyses of precipitation data from
1982 to 2007 show that the MAP within these regions is higher than 1200 mm (Ding et
al., 2014).

Regional vegetation has clear vertical zonation, which mainly consists of small-
leaf, arid shrubs at 1300–2200 m a.s.l., mixed broadleaf-conifer forests, evergreen and
deciduous broad-leaved mixed forests at 2000–2800 m a.s.l., *Picea* and *Abies* forests
at 2800–3600 m a.s.l., and alpine shrubs and meadows at > 3600 m a.s.l. (Ma et al.,
2004; ~~Zhang et al., 2008~~). There are two key factors that influence vegetation
distribution and ecological conditions in the study area: the arid and windy climate,
which has a large temperature difference between day and night, and tectonics activity
characterized by frequent earthquakes (Lin, 2008; Wang et al., 2011). For example,
strong earthquakes often induce landslides that can destroy vegetation cover in the study

area (Xu et al., 2012, 2014). Both of these factors lead to fragility in landscape and vegetation cover.

2.2 Segmented characteristics of the Min River

Based on the topographical and geomorphological characteristics, fault and vegetation distribution patterns, the upper Min River could be subdivided into four segments (Fig. 1b).

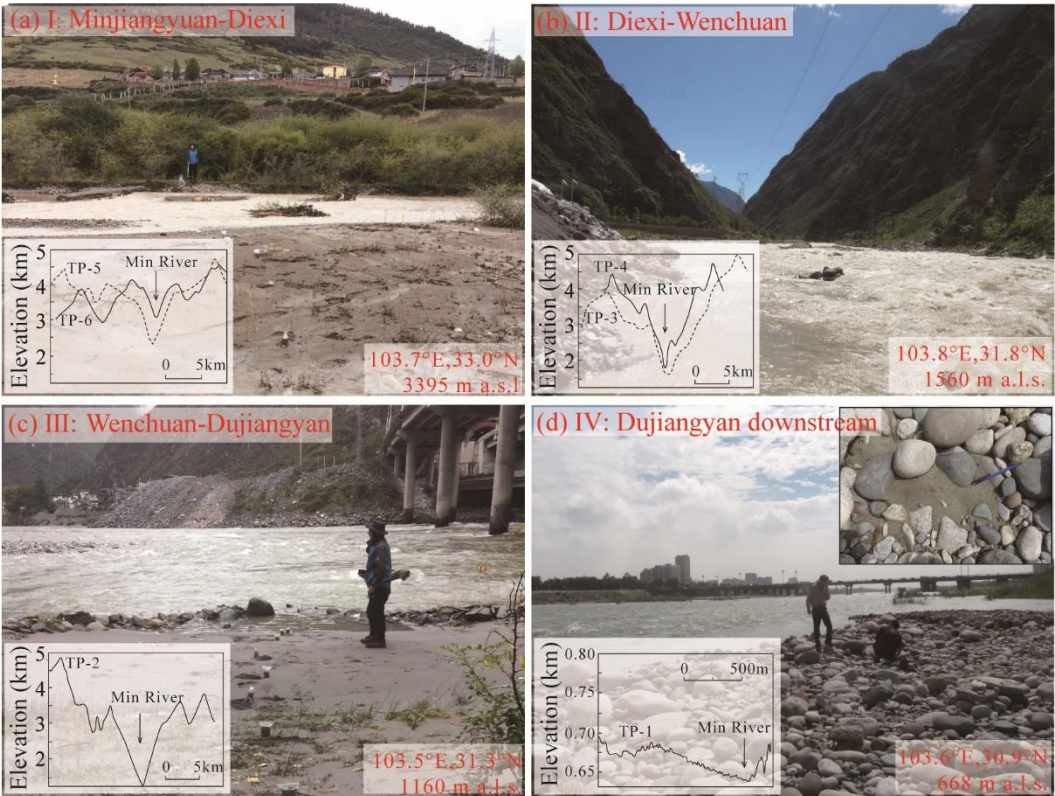


Figure 2 Photographs of field sampling sites in the upper Min River. The locations of cross-sections through the Min River valleys (Zhang et al., 2005) are shown in Fig. 7c.

Segment I is the Minjiangyuan — Diexi segment (3460–2190 m a.s.l.). The riverbed in this segment is directly connected with one side of the Min Mountain and has a valley bottom width of 200–1000 m (Zhang et al., 2005) (Fig. 2a). Downstream from Minjiangyuan, valley bottom width narrows markedly and is only 200–300 m in Zhenjianguan — Diexi segment (Zhang et al., 2005). The relative relief of the Min

Mountain increases significantly from Minjiangyuan to Diexi along the Min River, especially from Zhenjiangguan to Diexi (Zhang et al., 2005). The vegetation coverage along this segment gradually deteriorates, with *Picea*, *Abies*, shrubs, and herbs in the Minjiangyuan — Songpan segment, but only a small number of shrubs and herbs in the Songpan — Diexi segment. Bedrock is widely exposed in the lower part of the segment. In this region, the monthly maximum wind speed reaches 15.4 m/s in Songpan.

Segment II is the Diexi — Wenchuan segment (2190–1470 m a.s.l.). The valley bottom width in this segment decreases to 200–300 m (Zhang et al., 2005), and the Min Mountains always occur in direct contact with the riverbed of the Min River (Fig. 2b). The longitudinal slope (12.6‰) reaches its maximum ~~regional value~~ near Diexi (Zhang et al., 2005). The regional vegetation coverage is mostly sparse and the bedrock is well exposed.

Segment III is the Wenchuan— Dujiangyan segment (1470–900m a.s.l.). The valley bottom width in this segment widens to about 200–500 m (Zhang et al., 2005) (Fig. 2c) and regional vegetation cover increases compared to segment II. In particular, the hillside around the Zipingpu Reservoir is covered with thick broad—leaved trees and herbs. The monthly maximum wind speed in Lixian is 14.0 m/s.

Segment IV is the Dujiangyan downstream — segment (900 – 630 m a.s.l.). This segment flows into the interior of the Sichuan Basin, where it has flat geomorphological features (i.e., the riverbed width is greater than 300 m; Fig. 2d), and then transitions into the middle reach of the Min River. The monthly maximum wind speed in Dujiangyan is 13.8 m/s.

3 Materials and methods

3.1 Field sampling and grain—size analysis

A ~340 km transect along the upper Min River was conducted during October 2017, starting in the eastern TP (Minjiangyuan, 33°01'59"N, 103°42'42"E; 3462 m a.s.l.) and ending in the Sichuan Basin (Dujiangyan, 30°56'25"N, 103°38'14"E; 634 m a.s.l.) (Fig. 1b). A total of 181 river samples were collected for grain-size analysis at 25 sites (Table S1). Sampling sites were selected from exposed, freshly-developed depositional sequences that occurred close to the active channel and its margins (Fig. 2). Voluminous bedrock gravel occurs around the sampling sites (Fig. 2). To ensure sample consistency associated with uniform flow regimes, each sample was collected at a depth of 0–0.2 m from different ~~places with~~ locations in each sampling sequence. All locations were carefully chosen to avoid contamination from riverbank materials or from anthropogenic reworking.

Grain-size analysis was conducted using a Malvern Mastersizer 3000 laser grain-size analyzer at the State Key Laboratory of Earthquake Dynamics, Institute of Geology, China Earthquake Administration in Beijing, China. About 0.5 g of sediment was pretreated with 20 ml of 30% H₂O₂ to remove organic matter and then with 10 ml of 10% HCl to remove carbonates. About 300 ml of deionized water was added, and the sample solution was kept for 24 h to rinse acidic ions. The sample residue was dispersed with 10 ml of 0.05 M (NaPO₃)₆ on an ultrasonic vibrator for 10 min before grain-size measurements. For each sample, the grain-size analyzer automatically outputs the median diameter (Md) and the percentages of each size fraction, with a relative error of less than 1%. Magnetic susceptibility (SUS) was measured using a Bartington MS2 susceptibility meter.

3.2 Y values

Mean grain size (Ms), standard deviation (σ), skewness (Sk), and kurtosis (K_G) are commonly used to discriminate ~~between~~ different depositional processes and environments. Sahu (1964) distinguished aeolian processes from those that operate in a littoral environment by using the following equation:

$$Y = -3.5688 Ms + 3.7016 \sigma^2 - 2.0766 Sk + 3.1135 K_G \quad (1)$$

Here, Y values less than -2.74 indicate an aeolian provenance and Y values greater than -2.74 indicate a hydrogenic provenance (Sahu, 1964). Calculated Y values for lacustrine sediments (Jiang et al., ~~2017~~2014, ~~2014~~2017), red clay, and loess—paleosol deposits (Lu and An, 1999; Wu et al., 2017; ~~Lu and An, 1999~~) are less than -2.74 , indicating an aeolian provenance.

3.3 End—member analysis

Numerical unmixing of grain—size distribution data into constituent components, known as end—member analysis (EMA), can yield valuable information about transport dynamics (Weltje, 1997; Paterson and Heslop, 2015; Jiang et al., 2017). According to the principle that the end—member number (EM) should be as small as possible (Weltje et al., 1997), several EMs obtained by end—element analysis imply that numerous dynamic mechanisms occurred during formation of these deposits. Generally, larger values of EMs correspond to a stronger transport capacity, which—~~itself~~ indicates different provenances (Vandenberghe, 2013; Dietze et al., 2014; Jiang et al., 2017). For instance, the peak values of EMs in Lixian lacustrine sediments were concentrated at $10 \mu m$ (EM_1) and $40 \mu m$ (EM_2), ~~and so reflect~~ing the background deposition of dust and locally sourced deposition transported by ambient wind, respectively (Jiang et al.,

2017). We analyzed the Min River samples using the AnalySize software for processing and unmixing grain-size data (Paterson et al., 2015), with parameters selected from the generalized Gaussian skewness model (SGG) (Egli, 2003).

3.4 Analysis of C-M and F-M diagrams

The analysis of C-M and F-M diagrams is useful to interpret sediment transport dynamics (Passega, 1957; Singh et al., 2007). In these diagrams, C is the coarsest percentile of the grain-size distribution in samples (one percentile), and M is the median diameter of the grain-size distribution, which are both indicators of the maximum and average transport capacity, respectively (Passega, 1957; Singh et al., 2007; Bravard et al., 2014). In addition, F represents the percentage of fractions finer than 125 μm (Singh et al., 2007). All values are plotted on a logarithmic scale, which produces specific patterns for distinct reaches (Singh et al., 2007; Bravard et al., 2014). A C-M diagram (Fig. S1) has the following sections: NO, rolling; OP, rolling with some grains transported in suspension; PQ, graded suspension with some grains transported by rolling; QR, graded suspension; RS, uniform suspension; and T, pelagic suspension (Passega, 1957; Bravard and Peiry, 1999; Bravard et al., 2014).

4 Results

4.1 Characteristics of grain-size and SUS

The median grain size (Md), five grain-size fractions (0-2 μm , 2-20 μm , 20-63 μm , 63-250 μm , >250 μm), SUS and Y values of the fluvial sediments Min River sediment can be divided into four segments/categories (Fig. 3), which correspond to the

different segments of the upper Min River (I – IV) defined above. The average values of Md increased significantly at Diexi (from 31.0 μm to 80.8 μm) and Wenchuan (from 49.3 μm to 170.2 μm), and decreased slightly at Dujiangyan (from 220.4 μm to 119.2 μm). The variations at these three sites are the most significant within the whole river (Table 1, Fig. 3).

Table 1 Statistics for grain-size fractions in the upper Min River.

Segments	Md (μm)	Percentage composition / (%)					SUS
		0–2	2–20	20–63	63–250	>250	
		μm	μm	μm	μm	μm	
I	31.0	2.8	40.3	27.1	23.7	6.2	11.6
II	80.8	0.4	25.3	20.3	34.6	19.4	11.3
III	170.2	0.3	20.0	13.9	31.9	33.8	193.5
IV	145.2	0.5	13.0	9.5	59.5	17.5	251.8

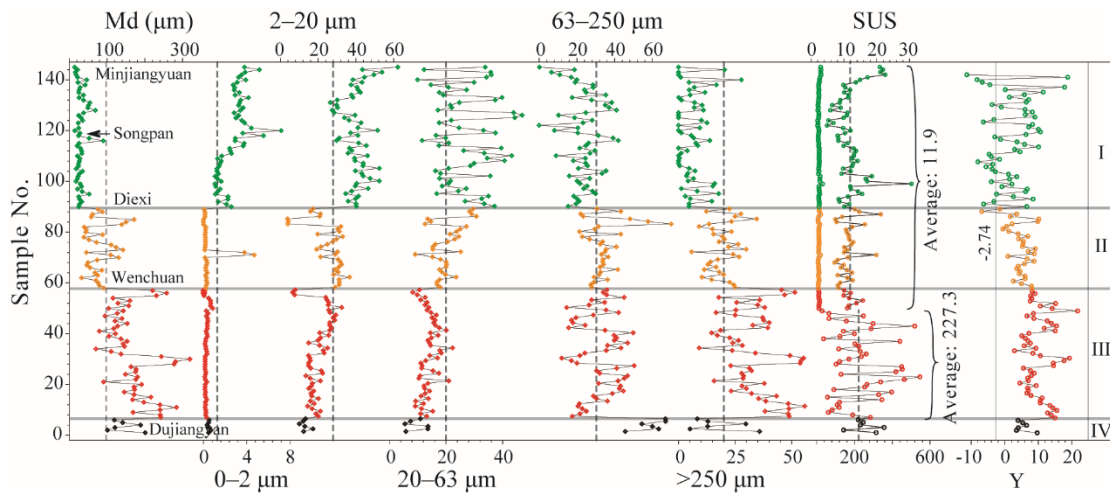


Figure 3 Variation of grain-size components and river sediment parameters from the upper Min River. The dotted lines represent the average value of the whole sequence.

Along the upper Min River downwards, the mean proportion of the 2–20 μm (I = 40.3%, II = 25.3%, III = 20.0%, and IV = 13.0%) and 20–63 μm fractions (I = 27.1%, II = 20.3%, III = 13.9%, and IV = 9.5%) exhibit a stepwise decrease (Table 1, Fig. 3).

The 63–250 μm fraction exhibits a sharp increase from segment I (23.7%) to II (34.6%) and from segment III (31.9%) to IV (59.5%), but a relatively minor change from segment II (34.6%) to III (31.9%) (Table 1, Fig. 3). The > 250 μm fractions exhibit a stepwise increase ~~between-from~~ segments I ~~to III, II, and III~~ (6.2%, 19.4%, and 33.8%, respectively), and a significant decrease from segment III (33.8%) to IV (17.5%) (Table 1, Fig. 3). ~~Measured~~-SUS values remained low in segments I (5.3–30.6, ~~with a mean of~~ 11.6) and II (7.1 to 21.2, ~~with a mean of~~ 11.3), but were significantly higher in segment III (9.9–546.5, ~~with a mean of~~ 193.5) and reached consistently high values in segment IV (142.1–356.5, ~~mean: 251.8~~) (Table 1, Fig. 3).

4.2 End-member analysis

Three end-members (EMs) ($R^2 = 0.93$) were identified in the Min River samples (Fig. 4) with peaks of 21.2 μm (58.0%), 185.8 μm (24.2%), and 351.7 μm (17.8%), respectively. Along the upper Min River downwards, these three EMs show clear stepwise changes between segments (Fig. 5). EM₁ shows a stepwise decrease (I = 82.5%, II = 53.1%, III = 38.6%, and IV = 23.7%), corresponding to the sum of the 2–20 μm and 20–63 μm fractions (Figs. 3, 5). EM₂ shows a sharp increase from segment I (13.1%) to II (31.4%) and from segment III (27.1%) to IV (67.4%), and a relatively smaller change from segment II (31.4%) to III (27.1%), corresponding to the 63–250 μm fraction. By contrast, EM₃ corresponds to the >250 μm fraction (Figs. 3, 5) and shows a stepwise increase ~~from between~~ segments I ~~to III, II, and III~~ (4.4%, 15.5% and 38.6%, respectively), and a significant decrease from segment III (38.6) to IV (23.7%).

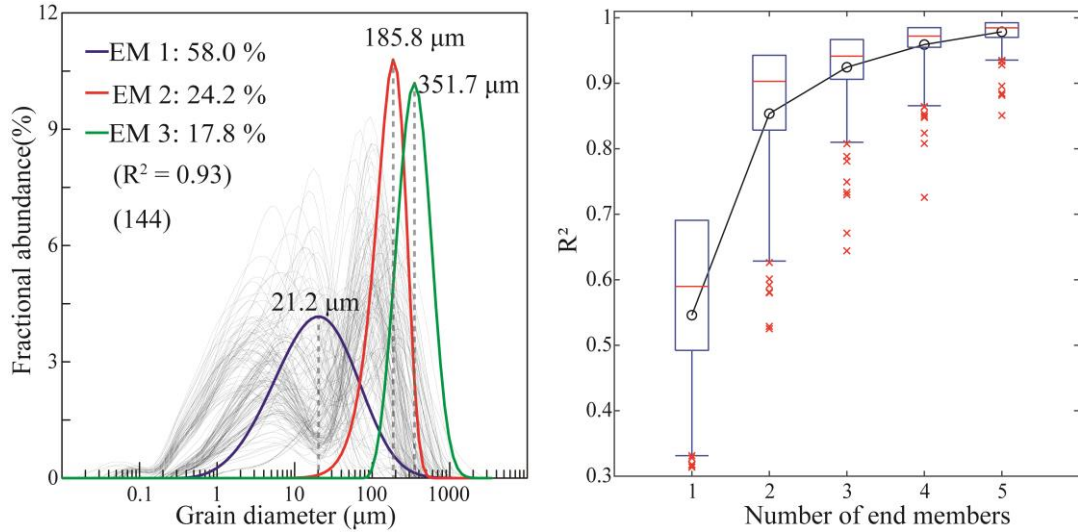


Figure 4 End-member analysis model of fluvial sediments from the upper Min River.

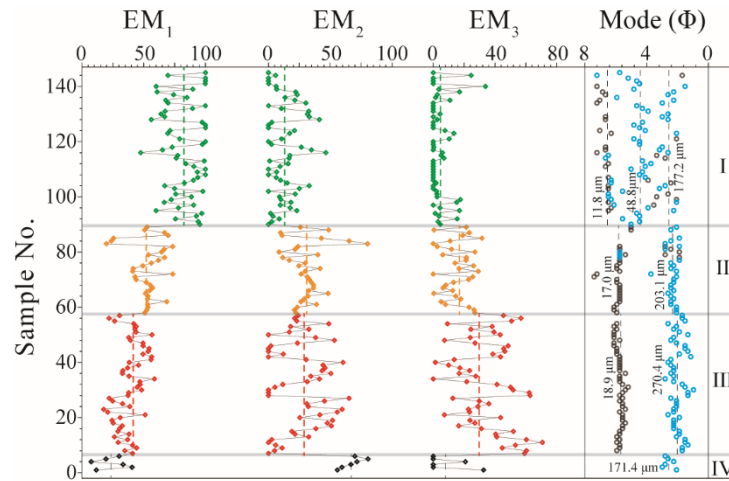


Figure 5 Variability of EMs and mode values of fluvial sediment samples collected from the upper Min River. The peak values (mode values) with $>1\%$ fractional abundance of the grain-size frequency distributions were extracted after consideration of a 1% instrumental error. Blue and gray circles represent the main and secondary peak modal values, respectively. The dotted lines represent the average value.

4.3 Characteristics of the grain-size frequency distribution

The grain-size frequency of river samples from segment I has a discrete distribution (Fig. S2) with three mode values at $\sim 11.8 \mu\text{m}$, $\sim 48.8 \mu\text{m}$, and $\sim 177.2 \mu\text{m}$. The main mode value of segment I occurred in the $\sim 48.8 \mu\text{m}$ portion. The grain-size

frequency distribution for segments II and III is strongly bimodal (Fig. S2), with the major and minor mode values at $\sim 203.1 \mu\text{m}$ and $\sim 17.0 \mu\text{m}$ for segment II, and $\sim 270.4 \mu\text{m}$ and $\sim 18.9 \mu\text{m}$ for segment III. The grain-size frequency distribution for segment IV is unimodal (Fig. S2) with a mode value of $\sim 171.4 \mu\text{m}$.

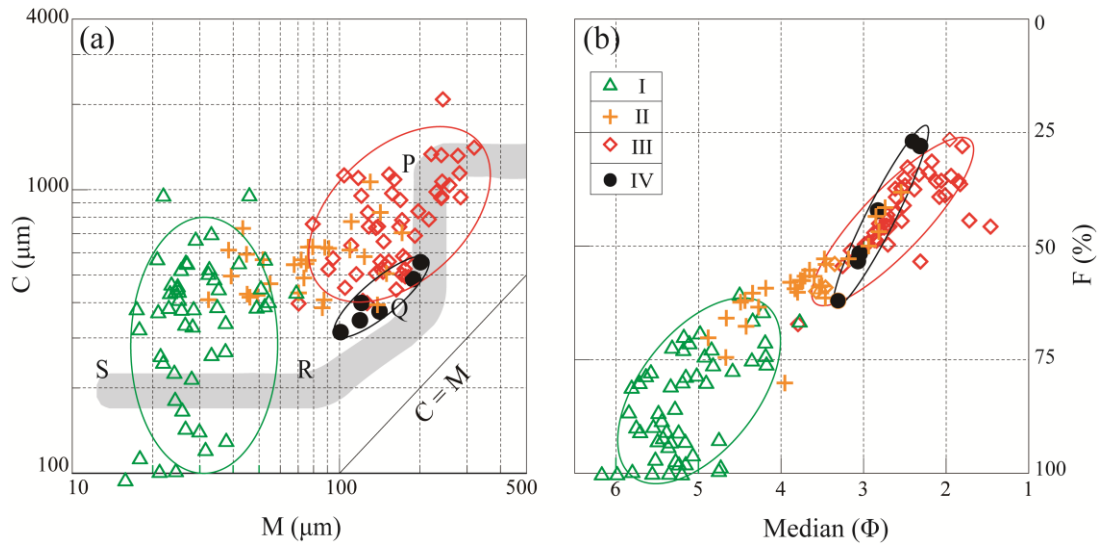


Figure 6 C-M and F-M diagrams distributions of fluvial sediment samples collected from the upper Min River.

4.4 C-M and F-M diagrams

On the C-M diagram for the Min River, samples from segment I are completely separate from those collected from segments III and IV. Most samples in segment II overlap with those of segment III (Fig. 6a). Among them, the M value of segment I ($13.9\text{--}89.8 \mu\text{m}$) mainly belongs to the RS section (Fig. 6a), although the C values exhibit a large variation between $54.8 \mu\text{m}$ and $964.3 \mu\text{m}$. Samples from segment II are distributed throughout the P-Q-R sections (Fig. 6a), have with C values of $383.5\text{--}1066.0 \mu\text{m}$, and M values of $32.2\text{--}171.4 \mu\text{m}$. Samples from segment III are concentrated

in the PQ section (Fig. 6a), ~~have with~~ C values of 396.9–2083.8 μm , and M values of 70.3–319.1 μm . Samples in segment IV plot close to the RQ section and are distributed parallel to the C = M line (Fig. 6a). ~~Fluvial sediments~~~~Samples collected from segments~~ of the Min River show similar distribution features in F–M diagrams to those ~~shown~~ in C–M diagrams (Fig. 6).

5 Discussion

5.1 Dynamic and provenance implications of fluvial sediments

Grain-size fractions, EMs, and mode values in different segments along the upper reaches of Min River reflect the distinct provenance and transport dynamics of fluvial sediments (McKinney and Sanders, 1978; Sun et al., 2002, 2004; Sun et al., 2007; ~~Vandenberghe, 2013~~; Dietze et al., 2014; ~~Vandenberghe, 2013~~). The EM₁ in segment I reaches a proportion of 82.5%, which corresponds to the fine particle components (<63 μm fractions). Previous studies have indicated that fractions with sizes of <10 μm and 10–40 μm represent background particles and regional dust that have been transported by wind (Dietze et al., 2014; Jiang et al., 2014, 2017), which contribute 51±11% and 42±14% of the lacustrine sediments across the TP, respectively (Dietze et al., 2014). Therefore, the EM₁ (fine-grained fractions) in segment I probably have an aeolian provenance. This inference is supported by five separate lines of evidence: 1) Md varies ~~within the in a~~ narrow range ~~of~~ 13.9 ~~to~~ –89.8 μm (Fig. 3), although the C values fluctuate widely between 54.8 μm and 964.3 μm (Fig. 7); 2) the distribution of samples in ~~an~~ RS section ~~in a of the~~ C–M diagram (Fig. 6) reflects uniform suspension, which likely

requires transportation by ubiquitous and strong wind (Fig. S1, Passega, 1957); 3) nearly half of the samples (i.e., 22 out of 55) have Y values of less than -2.74 , which is indicative of an aeolian origin (Sahu, 1964); 4) loess deposits are widely distributed in the study area, especially from Diexi upstream (Fig. S3) (Liu et al., 2013; Shen et al., 2017), ~~which-and-may~~ represent a voluminous source of dust particles; and 5) the study area has a high mean altitude of 2840 m, and the monthly maximum wind speed can reach 15.4 m/s, which ~~is conducive to would allow for~~ strong aeolian transport.

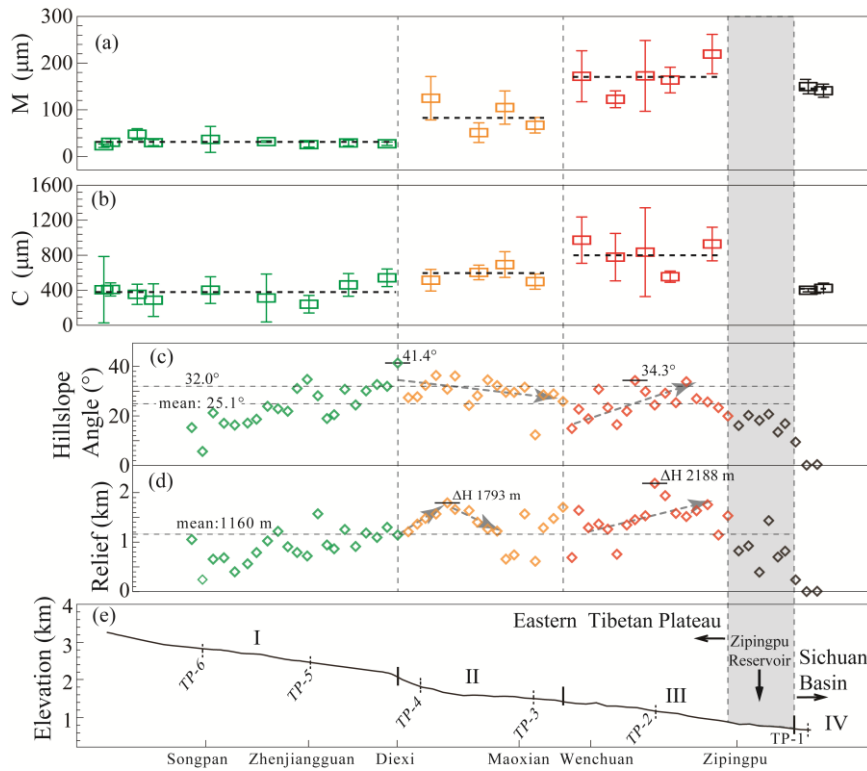


Figure 7 Variation characteristics of (a) M and (b) C values of the grain-size index. (c) Riverbed base-level and the position of the cross-section of the upper Min River (Zhang et al., 2005). (d) Hillslope angle and (e) local relief along the upper Min River. A 4*4 km grid was delineated along the upper Min River (~260 km). The highest ridgeline and riverbed height in the grid were extracted from a DEM map, and the local

relief was then obtained by calculating the highest ridgeline minus the riverbed height.

The hillslope angle was obtained by solving for tan (local relief/slope length).

The EM₂ in segment IV reaches the highest value (185.8 μm ; 67.4%) ~~recorded in~~ of the whole sequence and corresponds to the 63–250 μm fraction (59.5%), which is consistent with previous studies ~~having~~ shown that fluvial deposits are composed mainly of a medium-sand component (modal size: 200–400 μm) (Middleton, 1976; Tsoar and Pye, 1987; Bennett and Best, 1995; Dietze et al., 2014). In the C–M diagram, sample data that lie close to the C = M line reflect the suspension transport of riverbed sediments (Fig. 6a) (Passega, 1957; Singh et al., 2007; ~~Passega, 1957~~). In addition, the single peak mode (Fig. S2d) of segment IV represents ~~a single~~ the river transport process and sedimentary environment (McKinney and Sanders, 1978), and the small ~~size~~ range of the grain-size frequency distribution also reflects a well-sorted effect of fluvial transport ~~product that was deposited by fluvial action~~ (Sun et al., 2002). Therefore, the EM₂ mainly reflect typical fluvial sediments.

EM₃ corresponds to the coarsest grain-size components (>250 μm) and has the highest value (351.7 μm ; 38.6%) of the whole sequence in segment III. The maximum values of C and M (Figs. 7a, b) in segment III indicate that it had the highest transport capacity (Passega, 1957; Singh et al., 2007; Bravard et al., 2014). Therefore, EM₃ represents the local sedimentary component ~~that was locally~~ transported over short distances (Dietze et al., 2014; Jiang et al., 2014, 2017). ~~The distribution characteristics of~~ Samples from segment III are in the PQ section in C-M diagram (Fig. 6a), indicating ~~that~~ dominant rolling and jumping transportation processes (Passega, 1957).

Meanwhile, the SUS values in segment III increase ~~to abnormally high values (28.5–546.5, with a mean of 227.3)~~ abruptly near ~~to~~ exposures of the Pengguan complex (Fig. ~~1a~~ 28.5–546.5, mean 227.3), although lower SUS values occur in the surrounding area (e.g., Zagunao River: 9.1–114.1, ~~with a mean of~~ 34.1, Fig. S4; Zipingpu reservoir: 5–60, Zhang et al., 2019; and segments I and II: 5.3–30.6, mean 11.5, Fig. 3). The precipitation in segment III is generally low (400–700 mm/a) and only significantly increases near ~~to~~ the Zipingpu reservoir (1200 mm/a), so that the sedimentary changes ~~were~~ muted until 2 years after the Wenchuan earthquake (Zhang et al., 2019) (Fig. 1b). In addition, the mean grain size in segment III (170.2 μm) increases before the Zagunao River (mean ~~of~~ 83.1 μm , Fig. S4) joins the Min River (Fig. 1b. 3), so and contribution from the Zagunao River can be precluded. Therefore, the abnormally high ~~grain-grain-~~ size and SUS values in segment III are likely caused by a local provenance change. Based on the indicative significance of EMs, combined with the regional climatic and tectonic background, the main control mechanisms of river sediment variation in different segments of the upper Min River are discussed below.

5.2 Climate controlled fine-grained fluvial sediments

The windy and semi-arid climate in the study area is responsible for more fine particle components (EM_1) in segment I (Jiang et al., 2014), which caused EM_1 ~~to~~ gradually decrease downstream as the wind weakens (Fig. 5). The relatively low precipitation (400–700 mm/a) and low runoff ($18.4\text{--}43.4 \times 10^8 \text{ m}^3$) (Fig. 1b) in segment I reflect the limited transport capacity of the river, and the angular gravels on the riverbed also indicate weak scouring, which preserves more fine-grained components

(EM₁) in fluvial sediments. Segment I developed along the Minjiang Fault (Fig. 1a), which has a low slip rate (0.30–0.53 mm/a, Kirby et al., 2000; Zhou et al., 2000, 2006; Tan et al., 2019) and therefore a weak influence on local provenance supply (Jiang et al., 2014, 2017). In addition, the wide riverbed (Fig. 2a), relatively low hillslope angle, and local relief in the Minjiangyuan – Songpan segment (Figs. 7d, e) causes *in situ* retention of locally sourced coarse components. Therefore, EM₂ and EM₃ make only a minor contribution to the fluvial sediments in segment I.

Segment IV is located inside the Sichuan Basin and is completely unaffected by alpine valleys in the eastern TP. It is characterized by a wide and flat geomorphological surface (Fig. 2d). The significant downstream increase in precipitation and runoff in the Zipingpu reservoir (Fig. 1b) indicates that fluvial action was the main control on sediment transportation in segment IV. In addition, well-rounded pebbles (Fig. 2d) on the riverbed prove this point.

5.3 Coarse-grained deposits controlled by tectonism

Fluvial sediments coarsen at the transition between segments I and II, highlighting an increase in EM₂ and EM₃ content, and a higher M value (Figs. 3, 7). This locality occurs at the intersection of the Minjiang Fault and the Songpinggou Fault (Fig. 1a), which was the epicenter of the Diexi *M*_s 7.5 earthquake in 1933 (Chen et al., 1994; Ren et al., 2018). As a result, the outcropping bedrock was severely damaged and so provided new, fresh, and local sediment sources (EM₃). Downstream from Diexi, field surveys exhibit that the altitude decreases by 400 m over a horizontal distance of 20 km, such that the longitudinal slope of the riverbed (12.6‰, Fig. 7c, Zhang et al., 2005) and the hillslope angle (41.4°, Fig. 7d) are highest in this region when compared to the entire

study area, which imply a higher regional denudation rate forced by active tectonics (Zhang et al., 2005; Whittaker et al., 2007a). These remarkable changes of geomorphology correspond well to a twofold increase in erosion coefficients that occur within 15 km of major faults in the eastern TP (Kirkpatrick et al., 2020) and more intense denudation at the location of seismogenic faulting along high-relief plateau margins (Li et al., 2017). The narrow valley and direct contact between the riverbed and hillside on either side in segment II (Fig. 2b) provide favorable conditions for rolling and jumping transportation of sediment along the hillslope. In addition, the rapid rising of the base-level of the Min River in segment II enhances the river's cutting and transport capacity (Merritts and Vincent, 1989; Stokes et al., 2002; Cheng et al., 2004; Whittaker et al., 2007a; Boulton et al., 2014).

EM₃ rapidly reaches its maximum fluctuation range in segment III (Fig. 5), likely due to the maximum transport force (C value) in the area (Fig. 7). The regional precipitation in segment III is low (400–700 mm/a) and only significantly increases near the Zipingpu reservoir (1200 mm/a) (Fig. 1b). From a tectonic perspective, the Maoxian–Wenchuan Fault, with a large-high dextral slip rate (1.0–3.8mm /a; Chen and Li, 2013; Wang et al., 2017) and a large-vertical slip rate (~1–2 mm/a; Liu et al., 2015), mainly controls the grain-size distribution of segment III (Fig.1). Previous studies have shown that the Maoxian – Wenchuan Fault occurs at a band of maximum exhumation along the eastern Longmen Shan Fault zone since the late Miocene (Tan et al., 2019). Therefore, rapid regional uplift and denudation rates (Kirby et al., 2002; Liang et al., 2013) not only generated a larger hillslope angle (mean value of 24.9°) and the highest local relief (2188 m), but also provided widespread source of fresh, coarse-grained,

and local sediment (Whittaker et al., 2007b, 2010) in segment III. ~~The significant coarsening of fluvial sediment at the beginning of segment III indicates the catchments undergoing a transient response to tectonics are associated with significant volumetric export of material.~~ At the beginning of segment III, the river sediments become significantly coarser, indicating a transient response to the tectonics, manifested by a large amount of material output (Whittaker et al., 2010). Moreover, the PQ distribution of segment III ~~samples~~ in the calculated C–M diagram (Fig. 4) shows the importance of rolling and jumping transport mechanisms (Passega, 1957), which correlate with the steep landform features in segment III (Fig. 2c). Exposures of hard Mesozoic granites instantaneously provide a local source of coarse components, and thus correspond to the maximum M and C values. Although regional climate generally has a weak influence on the supply of coarse particles, the concentrated distribution of particles within the calculated grain–size frequency distribution (Fig. S2c) indicates that fluvial action played an effective role in sorting local sediment sources (Sahu, 1964; Sun et al., 2002; Frings, 2008). The persistent occurrence of the coarsest grain–size across the segment III responds to the fact that the catchments crossing faults maintain their high slip rate over time, which exhibits a sharp contrast to that of segment I.

Generally, a large earthquake is followed by a period of enhanced mass wasting and fluvial sediment evacuation (Hovius et al., 2011; Wang et al., 2015). The Wenchuan M_s 8.0 earthquake in 2008 caused severe geomorphological damage in this region, and the annual average suspended sediment flow in regional rivers increased by a factor of 3–7 following the earthquake. The river recovered to its pre–earthquake level just 1.2

± 0.9 years later (Wang et al., 2015). However, over 70% of the co-seismic debris has stabilized in place along the hillslopes during the following decades (Dai et al., 2021) and will take 370 years to be removed out of the mountains (Wang et al., 2017). The above results are sufficient to show that the extensive existence of gravel in Min River can reveal tectonic activity for a long time. However, these studies cannot explain the relatively fine fluvial and wind transport characteristics. As suchIn addition, we believe that co-seismic debris generated by the Wenchuan earthquake in 2008 had negligible influence on our sample collection campaign conducted in 2017.

5.4 Geomorphic morphology reveals tectonic activity

Alpine valleys characterize the landscape of the upper reaches of the Min River in the eastern TP (Figs. 2, 7) and have an incision depth of 300–1500 m (Li et al., 2005; Zhang et al., 2005) (Fig. 6a). In segment I, hillslope angles and local relief gradually increase downstream along the Minjiang Fault from 5° to 34.8° and 243 m to 1572 m, respectively (Fig. 7d, e). However, these changes seem to be decoupled with the high and stable proportion of fine-grained background dust in the fluvial sediments of segment I (Figs. 3, 5), which is an open and interesting question. The consistent precipitation and runoff rates explain the calculated consistency in transport power, as defined by unchanging values of C and M (Fig. 7). We note that the longitudinal slope of the riverbed (6.7–7.6‰, Fig. 7c; Zhang et al., 2005) in segment I steadily changes as altitude decreases from 3460 m to 2190 m; therefore, gradual steepening of the landscape is likely a response to enhanced river-related erosion (Merritts and Vincent, 1989; Stokes et al., 2002; Cheng et al., 2004). The high vegetation density in the

Minjiangyuan — Songpan region is also probably modulated by the lower topographic slope (Figs. 2a, 7) (Olen et al., 2016). These are consistent with generally weak activity of the Minjiang Fault (Kirby et al., 2000; Zhou et al., 2000, 2006; Tan et al., 2019).

In segment II, the hillslope angle ($12.3\text{--}41.4^\circ$, with a mean of 30.1°) is generally steeper than the average for the whole study area (25.1°), and the highest angles (41.4°) far exceed the stability threshold of $\sim 32^\circ$ for landslide denudation, which suggests that landslide-dominated hillslope denudation has kept pace with the rates of rock uplift and valley incision in segment II (Burbank, et al., 1996; Montgomery and Brandon, 2002; Clarke and Burbank, 2010; Wang et al., 2014). Along the studied transect, local relief in segment II initially increases and then decreases (Fig. 7c), and the flow direction of the Min River also changes from roughly N—S to NW—SE (Fig. 1a). The lithology in segment II changes from Triassic to Silurian (Fig. 1a), and seismic activity transitions from the Minjiang Fault to the Maoxian — Wenchuan Fault. Given that segment II records the lowest annual rainfall in the study area (<500 mm/a, Fig. 1), this transformation of tectonic activity and lithology likely plays a dominant role on fluvial erodibility (Selby, 1980; Stokes et al., 2008; Whittaker et al., 2007a; Zondervan et al., 2020), and influences changes of regional geomorphology and river drainage.

Hillslope angles ($14.9^\circ\text{--}34.3^\circ$, ~~with a mean of~~ 24.9°) and local relief ($689\text{--}2188$ m, ~~with a mean of~~ 1463 m) in segment III exhibit a general increase along the Maoxian — Wenchuan Fault (Figs. 1, 7), although they differ from the increasing trends shown in segment I. For example, the highest local relief throughout the entire sequence occurs in segment III, although its mean hillslope angle (24.9°) is lower than the mean value

(25.1°) of the entire sequence (Fig. 7). In addition, precipitation and runoff only show a significant increase adjacent to the Zipingpu reservoir (Fig. 1). We note that the regional bedrock in segment III is ~~dominated by~~ hard Mesozoic granites of the Pengguan complex (Fig. 1a), and that the Maoxian–Wenchuan Fault is situated on the zone of maximum exhumation along the Longmen Shan fault zone (Tan et al., 2019). Therefore, the higher local relief along segment III indicates that active Maoxian–Wenchuan Fault (Tan et al., 2019) caused enhanced rock uplift and valley incision (Whittaker et al., 2007a; Tan et al., 2019), which accounts for the largest transport forces (C values, Fig. 7) and the coarsest local components (EM₃, Fig. 5) in this section. Nevertheless, a decrease in the mean hillslope angle within segment III may be attributed to hardening of the exposed bedrock of the Pengguan complex rather than weakening of tectonic activity along the Maoxian–Wenchuan Fault. Even if the shortening rates are generally slow in the eastern TP (Densmore et al., 2008; Zhang, 2013), and satellite data may be equivocal (Kirby et al., 2008), grain-size analysis of fluvial sediments combined with topographic analyses can help guide the identification of regional tectonic activity effectively (Schoenbohm et al., 2004; Kirby et al., 2003, 2008; Schoenbohm et al., 2004; Tan et al., 2019).

6 Conclusion

Grain-size analysis was conducted on modern fluvial sediments of the upper Min River ~~and this information was integrated with vegetation, hydrology, geomorphology (local relief and hillslope) and geology (fault and lithology) data~~ to extract regional

~~climate and~~ tectonic signals in the eastern TP. Integrated with vegetation, hydrology, geomorphology (local relief and hillslope) and geology (fault and lithology) data, This procedure identified three segments of tectonic activity along the upper Min River were identified. The Minjiang Fault, situated in the Minjiangyuan — Diexi segment, generally shows weak tectonic activity. The Maoxian-Wenchuan Fault from Diexi ~~to~~ Wenchuan ~~to and from~~ Wenchuan ~~to~~ Dujiangyan segments shows enhanced ~~phase of regional~~ tectonic activity. However, the segment from Dujiangyan to the Sichuan ~~basin~~ Basin records almost no evidence of tectonic activity.

In this study, we report a new approach that can reveal the ~~style of~~ regional tectonic activity by analyzing fluvial sediments collected from tectonically active regions. The novelty of this research method and the reliability of the results ~~in this study~~ provide a key framework with which regional tectonic activity can be revealed through the study of fluvial sediments in other tectonically active localities worldwide.

Data availability

Data are available in the figshare database (<https://doi.pangaea.de/10.6084/m9.figshare.17111402>).

Author contributions

The paper was written by WS and HCJ with major contributions by HYX. SYM got geomorphic data. WS, HYX and SQZ participated in field surveys and sample collection. SQZ, JWF and XTW conducted laboratory tests and interpreted the results.

All authors reviewed and approved the paper.

Competing interests

The contact author has declared that neither they nor their co-authors have any competing interests.

Acknowledgements

This study was supported by the National Nonprofit Fundamental Research Grant of China, Institute of Geology, China Earthquake Administration (IGCEA2126 and IGCEA1906) and the Grant of the State Key Laboratory of Earthquake Dynamics, Institute of Geology, China Earthquake Administration (LED2022A06).—

References

- Beek, V.D., Bishop, P.: Cenozoic river profile development in the upper Lachlan catchment (SE Australia) as a test of quantitative fluvial incision models. *J. Geophys. Res. Solid Earth*, 108(B6), 2309, <https://doi.org/10.1029/2002JB002125>, 2003.
- Bennett, S.J., Best, J.L.: Mean flow and turbulence structure over fixed, two-dimensional dunes: implications for sediment transport and bedform stability. *Sedimentology*, 42(3), 491-513, <https://doi.org/10.1111/j.1365-3091.1995.tb00386.x>, 1995.
- Blanckenburg, F.: The control mechanisms of erosion and weathering at basin scale from cosmogenic nuclides in river sediment. *Earth Planet. Sci. Lett.*, 237, 462-479, <https://doi.org/10.1016/j.epsl.2005.06.030>, 2005.
- Boulton, S.J., Stokes, M., Mather, A.E.: Transient fluvial incision as an indicator of active faulting and Plio-Quaternary uplift of the Moroccan High Atlas. *Tectonophysics*, 633(1), 16-33, <https://doi.org/10.1016/j.tecto.2014.06.032>, 2014.

618 Bravard, J.P., Goichot, M., Tronchère, H.: An assessment of sediment-transport processes in the
619 Lower Mekong River based on deposit grain sizes, the CM technique and flow-energy data.
620 *Geomorphology*, 207, 174-189, <https://doi.org/10.1016/j.geomorph.2013.11.004>, 2014.

621 Burbank, D. W., Blythe, A. E., Putkonen, J., Pratt-Sitaula, B., Gabet, E., Oskin, M., Barros, A., Ojha,
622 T. P.: Decoupling of erosion and precipitation in the Himalayas. *Nature*, 426(6967), 652-655,
623 <https://doi.org/doi:10.1038/nature02187>, 2003.

624 Burbank, D.W., Fielding, E., Anderson, R.S., Brozovic, N., Reid, M. D.C., Leland, J.: Bedrock
625 incision, rock uplift and threshold hillslopes in the northwestern Himalayas. *Nature*, 379(6565),
626 505-510, <https://doi.org/10.1038/379505a0>, 1996.

627 Chen, H., Li, Y.: Water system responding to the dextral strike-slipping of the Longmen Shan fault
628 zone in the upper Min River basin. *J. Mount. Sci.*, 31(2), 211-217,
629 <https://doi.org/10.3969/j.issn.1008-2786.2013.02.010>, 2013 (in Chinese).

630 Chen, S.A., Michaelides, K., Grieve, S.W.D., Singer, M.B.: Aridity is expressed in river topography
631 globally. *Nature*, 573, 573-577, <https://doi.org/10.1038/s41586-019-1558-8>, 2019.

632 Chen, S.F., Wilson, C., Deng, Q.D., Zhao, X.L. Zhi, L.L.: Active faulting and block movement
633 associated with large earthquakes in the Min Shan and Longmen Mountains, northeastern
634 Tibetan Plateau. *J. Geophys. Res. Solid Earth*, 99(B12), 24025-24038,
635 <https://doi.org/10.1029/94JB02132>, 1994.

636 Chen, Z., Burchfiel, B.C., Liu, Y., King, R.W., Royden, L.H., Tang, W., Wang, E., Zhao, J., Zhang,
637 X.: Global positioning system measurements from eastern Tibet and their implications for
638 India/Eurasia intercontinental deformation. *J. Geophys. Res. Solid Earth*, 105(B7), 16215-
639 16227, <https://doi.org/10.1029/2000jb900092>, 2000.

640 Cheng, S.P., Deng, Q.D., Li, C.Y., Yang, G.Z.: Dynamical mechanism, physical erosion processes
641 and influence factors of fluvial incision: A review and prospect. *Quat. Sci.*, 24, 421-429,
642 <https://doi.org/10.3321/j.issn:1001-7410.2004.04.008>, 2004 (in Chinese).

643 Clapp, E.M., Bierman, P.R., Caffee, M.: Using ^{10}Be and ^{26}Al to determine sediment generation rates
644 and identify sediment source areas in an arid region drainage basin. *Geomorphology*, 45, 89-
645 104, [https://doi.org/10.1016/S0169-555X\(01\)00191-X](https://doi.org/10.1016/S0169-555X(01)00191-X), 2002.

646 Clapp, E.M., Bierman, P.R., Schick, A.P., Lekach, J., Enzel, Y., Caffee, M.: Sediment yield exceeds

- sediment production in arid region drainage basins, *Geology*, 28, 995-998,
[https://doi.org/10.1130/0091-7613\(2000\)28<995:SYESPI>2.0.CO;2](https://doi.org/10.1130/0091-7613(2000)28<995:SYESPI>2.0.CO;2), 2000.
- Clarke, B.A., Burbank, D.W.: Bedrock fracturing, threshold hillslopes, and limits to the magnitude
of bedrock landslides. *Earth Planet. Sci. Lett.*, 297(3-4), 577-586,
<https://doi.org/10.1016/j.epsl.2010.07.011>, 2010.
- Dai, F.C., Xu, C., Yao, X., Xu, L., Tu, X.B., Gong, Q.M.: Spatial distribution of landslides triggered
by the 2008 Ms 8.0 Wenchuan earthquake, China. *J. Asian Earth Sci.*, 40, 883-895,
<https://doi.org/10.1016/j.jseaes.2010.04.010>, 2011.
- Dai, L.X., Scaringi, G., Fan, X.M., Yunus, A.P., Liu, Z.J., Xu, Q., Huang, R.Q.: Coseismic debris
remains in the orogen despite a decade of enhanced landsliding. *Geophys. Res. Lett.*,
<https://doi.org/10.1029/2021GL095850>, 2021.
- Deng, Q.D., Cheng, S.P., Ma, J., Du, P.: Seismic activities and earthquake potential in the Tibetan
Plateau. *Chinese J. Geophys.*, 57(5), 2025-2042, <https://doi.org/10.1002/cjg2.20133>, 2014 (in
Chinese).
- Densmore, A. L., Ellis, M.A., Yong, L., Zhou, R., Richardson, N.: Active tectonics of the Beichuan
and Pengguan faults at the eastern margin of the Tibetan Plateau. *Tectonics*, 26(4), TC4005,
<https://doi.org/10.1029/2006TC001987>, 2008.
- Duvall, A., Kirby, E., Burbank, D.: Tectonic and lithologic controls on bedrock channel profiles and
processes in coastal California. *J. Geophys. Res. Earth Surface*, 109, F03002,
<https://doi.org/10.1029/2003JF000086>, 2004.
- Dietze, E., Maussion, F., Ahlborn, M., Diekmann, B., Hartmann, K., Henkel, K., Kasper, T., Lockot,
G., Opitz, S., Haberzettl, T.: Sediment transport processes across the Tibetan Plateau inferred
from robust grain-size end members in lake sediments. *Clim. Past*, 10, 91-106,
<https://doi.org/10.5194/cp-10-91-2014>, 2014.
- Ding, H.R., Ma, G.W., Ni, S.J., Shi, Z.M., Zhao, G.H., Yan, L., Yan, Z.K.: Study on sediment
discharge increase caused by Wenchuan earthquake landslide and heavy rainfall in the upper
reaches of the Min River. *J. Sichuan Univ.*, 46(3), 49-55,
<https://doi.org/10.15961/j.jsuese.2014.03.006>, 2014 (in Chinese).
- Egli, R.: Analysis of the field dependence of remanent magnetization curves. *J. Geophys. Res. Solid
Earth*, 108(B2), 1-26, <https://doi.org/10.1029/2002JB002023>, 2003.
- Frings, R.M.: Downstream fining in large sand-bed rivers. *Earth Sci. Rev.*, 87, 39-60,

678 <https://doi.org/10.1016/j.earscirev.2007.10.001>, 2008.

679 Hovius, N., Meunier, P., Lin, C.W., Chen, H., Chen, Y.G., Dadson, S., Horng, M.J., Lines, M.:
680 Prolonged seismically induced erosion and the mass balance of a large earthquake. *Earth Planet.*
681 *Sci. Lett.*, 304(3-4), 347-355, <https://doi.org/10.1016/j.epsl.2011.02.005>, 2011.

682 Jiang, H., Zhang, J., Zhang, S., Zhong, N., Wan, S., Alsop, G.I., Xu, H., Guo, Q., Yan, Z.: Tectonic
683 and climatic impacts on environmental evolution in East Asia during the Palaeogene. *Geophys.*
684 *Res. Lett.*, 49, e2021GL096832, <https://doi.org/10.1029/2021GL096832>, 2022.

685 Jiang, H.C., Shevenell, A., Yu, S., Xu, H.Y., Mao, X.: Decadal- to centennial-scale East Asian
686 summer monsoon variability during the Medieval Climate Anomaly reconstructed from an
687 eastern Tibet lacustrine sequence. *J. Paleolimnology*, 54, 205-222,
688 <https://doi.org/10.1007/s10933-015-9847-1>, 2015.

689 Jiang, H.C., Mao, X., Xu, H.Y., Yang, H.L., Ma, X.L., Zhong, N., Li, Y.H.: Provenance and
690 earthquake signature of the last deglacial Xinmocun lacustrine sediments at Diexi, East Tibet.
691 *Geomorphology*, 204, 518-531, <https://doi.org/10.1016/j.geomorph.2013.08.032>, 2014.

692 Jiang, H.C., Zhong, N., Li, Y.H., Ma, X.L., Xu, H.Y., Shi, W., Zhang, S.Q., Nie, G.Z.: A continuous
693 13.3-ka record of seismogenic dust events in lacustrine sediments in the eastern Tibetan Plateau.
694 *Sci. Rep.*, 7:15686, <https://doi.org/10.1038/s41598-017-16027-8>, 2017.

695 Jiang, H.C., Zhong, N., Li, Y.H., Xu, H.Y., Yang, H.L., Peng, X.P.: Soft sediment deformation
696 structures in the Lixian lacustrine sediments, Eastern Tibetan Plateau and implications for
697 postglacial seismic activity. *Sediment. Geol.*, 344, 123-134,
698 <https://doi.org/10.1016/j.sedgeo.2016.06.011>, 2016.

699 Kirby, E., Whipple, K.X., Burchfiel, B.C., Tang, W.Q., Berger, G., Sun, Z.M., Chen, Z.L.:
700 Neotectonics of the Min Shan, China: implications for mechanisms driving quaternary
701 deformation along the eastern margin of the Tibetan Plateau. *GSA Bull.*, 112(3), 375-393,
702 [https://doi.org/10.1130/0016-7606\(2000\)112<375:NOTMSC>2.0.CO;2](https://doi.org/10.1130/0016-7606(2000)112<375:NOTMSC>2.0.CO;2), 2000.

703 Kirby, E., Reiners, P.W., Krol, M.A., Whipple, K.X., Hodges, K.V., Farley, K.A., Tang, W.Q., Chen,
704 Z.L.: Late Cenozoic evolution of the eastern margin of the Tibetan Plateau: inferences from
705 $^{40}\text{Ar}/^{39}\text{Ar}$ and, U-Th/He thermochronology. *Tectonics*, 21(1), 1-20,
706 <https://doi.org/10.1029/2000TC001246>, 2002.

707 Kirby, E., Whipple, K. and Harkins, N.: Topography reveals seismic hazard. *Nat. Geosci.*, 1(8), 485-
708 487, <https://doi.org/10.1038/ngeo265>, 2008.

- Kirby, E., Whipple, K.X., Tang, W.Q. and Chen, Z.L.: Distribution of active rock uplift along the eastern margin of the Tibetan Plateau: Inferences from bedrock channel longitudinal profiles. *J. Geophys. Res. Solid Earth*, 108(B4), 2217, <https://doi.org/doi:10.1029/2001JB000861>, 2003.
- Kirkpatrick, H.M., Moon, S., Yin, A., Harrison, T.M.: Impact of fault damage on eastern Tibet topography. *Geology*, 48, <https://doi.org/10.1130/G48179.1>, 2020.
- Li, G., Westa, A.J., Densmoreb, A.L., Jin, Z.D., Zhang, F., Wang, J., Clark, M., Hilton, R.G.: Earthquakes drive focused denudation along a tectonically active mountain front. *Earth Planet. Sci. Lett.*, 472, 253-265, <https://doi.org/10.1016/j.epsl.2017.04.040>, 2017.
- Li, Y., Cao, S.Y., Zhou, R.J., Densmore, A.L., Ellis, M.: Late Cenozoic Minjiang incision rate and its constraint on the uplift of the eastern margin of the Tibetan plateau. *Acta Geol. Sinica*, 79(1), 28-37, <https://doi.org/10.3321/j.issn:0001-5717.2005.01.004>, 2005 (in Chinese).
- Li, Y.H., Jiang, H.C., Xu, H.Y., Liang, L.J.: Analyses on the triggering factors of large quantities of landslides in the upper reaches of the Minjiang River, Sichuan province. *Seism. Geol.*, 37(4), 1147-1161, <https://doi.org/10.3969/j.issn.0253-4967.2015.04.017>, 2015 (in Chinese).
- Liang, S.M., Gan, W.J., Shen, C.Z., Xiao, G.R., Liu, J., Chen, W.T., Ding, X.G., Zhou, D.M.: Three-dimensional velocity field of present-day crustal motion of the Tibetan Plateau derived from GPS measurements. *J. Geophys. Res. Solid Earth*, 118(10), 1-11, <https://doi.org/10.1002/2013JB010503>, 2013.
- Liang, L.J. and Jiang, H.C.: Geochemical composition of the last deglacial lacustrine sediments in East Tibet and implications for provenance, weathering and earthquake events. *Quat. Inter.*, 430, 41-51, <https://doi.org/10.1016/j.quaint.2015.07.037>, 2017.
- Liu, M.: Research on the risk stone under wind loading with wind tunnel test in the Min River Valley. Chengdu University of Technology, Sichuan, p. 10-38, 2014 (in Chinese).
- Lin, M.B.: The huge Wenchuan earthquake and Longmen tectonic belt. *J. Chengdu Univ. Technol.*, 35(4), 366-370, <https://doi.org/10.3969/j.issn.1671-9727.2008.04.004>, 2008 (in Chinese).
- Liu, W.M., Yang, S.L., Fang, X.M.: Loess recorded climatic change during the last glaciation on the eastern Tibetan Plateau, western Sichuan. *J. Jilin Univ. Earth Sci. Edi.*, 43(3), 974-982, <https://doi.org/http://ir.itpcas.ac.cn/handle/131C11/2852>, 2013 (in Chinese).
- Liu, X.X., Wu, Y.Q., Jiang, Z.S., Zhan, W., Li, Q., Wen, W.X., Zhou, Z.Y.: Preseismic deformation in the seismogenic zone of the Lushan Ms 7.0 earthquake detected by GPS observations. *Sci. China, Earth Sci.*, 45(9), 1198-1207, <https://doi.org/10.1007/s11430-015-5128-0>, 2015.
- Lu, H.Y., An, Z.S.: Comparison of grain-size distribution of Red Clay and Loess-paleosol deposits

in Chinese Loess Plateau. *Acta Sediment. Sinica*, 17(2), 226-232,
<https://doi.org/10.3969/j.issn.1000-0550.1999.02.011>, 1999.

Ma, K.M., Fu, B.J., Liu, S.L., Guan, W.B., Liu, G.H., Lu, Y.H., Anand, M.: Multiple-scale soil
 moisture distribution and its implications to ecosystem restoration in an arid river valley, China.
Land Degrad. Develop., 15(1), 75-85, <https://doi.org/10.1002/ldr.584>, 2004.

Ma, Y.W., Wang, G.Z., Hu, X.W.: Tectonic deformation of Pengguan complex as a nappe. *Acta Geol.*
Sichuan, 2, 110-114, 1996 (in Chinese).

Matmon, A., Bierman, P.R., Larsen, J., Southworth, S., Pavich, M., Caffee, M.: Temporally and
 spatially uniform rates of erosion in the southern Appalachian Great Smoky Mountains.
Geology, 31, 155-158, [https://doi.org/10.1130/0091-7613\(2003\)0312.0.CO;2](https://doi.org/10.1130/0091-7613(2003)0312.0.CO;2), 2003a.

Matmon, A., Bierman, P.R., Larsen, J., Southworth, S., Pavich, M., Finkel, R., Caffee, M.: Erosion
 of an ancient mountain range, the Great Smoky Mountains, North Carolina and Tennessee.
Amer. J. Sci., 303, 817-855, <https://doi.org/10.2475/ajs.303.9.817>, 2003b.

McKinney, G.M., Sanders, J.E.: *Principles of sedimentology*. Wiley, New York, No. of pages 792,
 1978.

Merritts, D., Vincent, K.R.: Geomorphic response of coastal streams to low, intermediate, and high
 rates of uplift, Medocino triple junction region, northern California. *GSA Bull.*, 101, 1373-
 1388, [https://doi.org/10.1130/0016-7606\(1989\)101<1373:GROCST>2.3.CO;2](https://doi.org/10.1130/0016-7606(1989)101<1373:GROCST>2.3.CO;2), 1989.

Middleton, G.V.: Hydraulic interpretation of sand size distributions. *J. Geol.*, 84(4), 405-426,
<https://doi.org/10.1086/628208>, 1976.

Molnar, P., Anderson, R.S., Anderson, S.P.: Tectonics, fracturing of rock, and erosion. *J. Geophys.*
Res. Earth Surface, 112, F03014, <https://doi.org/10.1029/2005JF000433>, 2007.

Montgomery, D.R., Brandon, M. T.: Topographic controls on erosion rates in tectonically active
 mountain ranges. *Earth Planet. Sci. Lett.*, 201(3), 481-489, [https://doi.org/10.1016/S0012-821X\(0200725-2](https://doi.org/10.1016/S0012-821X(0200725-2), 2002.

Najman, Y.: The detrital record of orogenesis: A review of approaches and techniques used in the
 Himalayan sedimentary basins. *Earth Sci. Rev.*, 74(1-2), 1-72,
<https://doi.org/10.1016/j.earscirev.2005.04.004>, 2006.

Nichols, K.K., Bierman, P.R., Caffee, M., Finkel, R., Larsen, J.: Cosmogenically enabled sediment

770 budgeting. *Geology*, 33(2), 133-136, <https://doi.org/10.1130/g21006.1>, 2005.

771 Olen, S.M., Bookhagen, B., Strecker, M.R.: Role of climate and vegetation density in modulating
 772 denudation rates in the Himalaya. *Earth Planet. Sci. Lett.*, 445, 57-67,
 773 <https://doi.org/10.1016/j.epsl.2016.03.047>, 2016.

774 Owen, L.A.: Tectonic geomorphology: a perspective. In: Shroder, J. (Editor in Chief), Owen, L.A.
 775 (Ed.), *Treatise on Geomorphology*. Academic Press, San Diego, CA, vol. 5, Tectonic
 776 Geomorphology, pp. 3-12, 2013.

777 Passega, R.: Texture as characteristic of clastic deposition. *Bull. Amer. Assoc. Petrol. Geol.*, 41,
 778 1952-1984, <https://doi.org/10.1306/0BDA594E-16BD-11D7-8645000102C1865D>, 1957.

779 Paterson, G.A., Heslop, D.: New methods for unmixing sediment grain size data. *Geochem.*
 780 *Geophys. Geosyst.*, 16(12), 4494-4506, <https://doi.org/info:doi/10.1002/2015GC006070>, 2015.

781 Perg, L.A., Anderson, R.S., Finkel, R.C.: Use of cosmogenic radionuclides as a sediment tracer in
 782 the Santa Cruz littoral cell, California, USA. *Geology*, 31, 299-302,
 783 [https://doi.org/10.1130/0091-7613\(2003\)031<0299:UOCRAA>2.0.CO;2](https://doi.org/10.1130/0091-7613(2003)031<0299:UOCRAA>2.0.CO;2), 2003.

784 Ren, J.J., Xu, X.W., Zhang, S.M., Yeats, R. S., Chen, J.W., Zhu, A.L., Liu, S.: Surface rupture of the
 785 1933 Ms 7.5 Diexi earthquake in eastern Tibet: implications for seismogenic tectonics.
 786 *Geophys. J. Inter.*, 212(3), 627-1644, <https://doi.org/10.1093/gji/ggx498>, 2018.

787 Riebe, C.S., Kirchner, J.W., Granger, D.E., Finkel, R.C.: Erosional equilibrium and disequilibrium
 788 in the Sierra Nevada, inferred from cosmogenic ²⁶Al and ¹⁰Be in alluvial sediment. *Geology*,
 789 28, 803-806, [https://doi.org/10.1130/0091-7613\(2000\)282.0.CO;2](https://doi.org/10.1130/0091-7613(2000)282.0.CO;2), 2000.

790 Riebe, S.R., Kirchner, J.W., Granger, D.E., Finkel, R.C.: Strong tectonic and weak climatic control
 791 of long-term chemical weathering rates. *Geology*, 29, 511-514, [https://doi.org/10.1130/0091-](https://doi.org/10.1130/0091-7613(2001)0292.0.CO;2)
 792 [7613\(2001\)0292.0.CO;2](https://doi.org/10.1130/0091-7613(2001)0292.0.CO;2), 2001.

793 Sahu, B. K.: Depositional mechanisms from the size analysis of clastic sediments. *J. Sediment. Res.*,
 794 34, 73-83, <https://doi.org/10.1306/74D70FCE-2B21-11D7-8648000102C1865D>, 1964.

795 Schoenbohm, L.M., Whipple, K.X., Burchfiel, B.C., Chen, L.: Geomorphic constraints on surface
 796 uplift, exhumation, and plateau growth in the Red River region, Yunnan Province, China. *GAS*
 797 *Bull.*, 116, 895-909, <https://doi.org/10.1130/B25364.1>, 2004.

798 Schumm, S.A., Khan, H.R.: Experimental study of channel patterns. *Nature*, 233(5319), 407-9,

799 <https://doi.org/10.1038/233407a0>, 1971.

800 Schumm, S.A., Khan, H.R.: Experimental study of channel patterns. *GAS Bull.*, 83(6), 1755-1770,

801 [https://doi.org/10.1130/0016-7606\(1972\)83\[1755:ESOCP\]2.0.CO;2](https://doi.org/10.1130/0016-7606(1972)83[1755:ESOCP]2.0.CO;2), 1972.

802 Selby, M.J.: A rock mass strength classification for geomorphic purposes, with tests from Antarctica

803 and New Zealand: *Zeitschrift für Geomorphologie*, v. 24, p. 31–51, 1980.

804 Shen, Y.Q., Guo, C.B., Wu, R.A., Ren, S.S., Su, F.R., Zhang, T.: Analysis on the development

805 characteristics and engineering geomechanical properties of the Songpan loess, western

806 Sichuan province, China. *J. Geomech.*, 23(5), 131-142, [https://doi.org/10.3969/j.issn.1006-](https://doi.org/10.3969/j.issn.1006-6616.2017.05.013)

807 [6616.2017.05.013](https://doi.org/10.3969/j.issn.1006-6616.2017.05.013), 2017 (in Chinese).

808 Shi, W., Jiang, H.C., Mao, X., Xu, H.Y.: Pollen record of climate change during the last deglaciation

809 from the eastern Tibetan Plateau. *PLOS ONE*, 15(5), e0232803,

810 <https://doi.org/10.1371/journal.pone.0232803>, 2020.

811 Shi, W., Jiang, H.C., Alsop, G.I., Wu, G.: A Continuous 13.3-Ka paleoseismic record constrains

812 major earthquake recurrence in the Longmen Shan collision zone. *Front. Earth Sci.*, 10:838299,

813 <https://doi.org/10.3389/feart.2022.838299>, 2022.

814 Singh, M., Singh, I.B., Müller, G.: Sediment characteristics and transportation dynamics of the

815 Ganga River. *Geomorphology*, 86(1/2), 144-175,

816 <https://doi.org/10.1016/j.geomorph.2006.08.011>, 2007.

817 Snyder, N., Whipple, K., Tucker, G., Merritts, D.: Landscape response to tectonic forcing: digital

818 elevation model analysis of stream profiles in the Mendocino triple junction region, northern

819 California. *GAS Bull.*, 112, 1250-1263, [https://doi.org/10.1130/0016-](https://doi.org/10.1130/0016-7606(2000)112<1250:LRTTFD>2.0.CO;2)

820 [7606\(2000\)112<1250:LRTTFD>2.0.CO;2](https://doi.org/10.1130/0016-7606(2000)112<1250:LRTTFD>2.0.CO;2), 2000.

821 Snyder, N.P. and Whipple, K.X.: Importance of a stochastic distribution of floods and erosion

822 thresholds in the bedrock river incision problem. *J. Geophys. Res. Solid Earth*, 108, 2117,

823 <https://doi.org/10.1029/2001JB001655>, 2003.

824 Stock, J. D., Dietrich, W. E.: Valley incision by debris flows: evidence of a topographic signature.

825 *Water Resour. Res.*, 39(4), ESG 1-1, <https://doi.org/10.1029/2001WR001057>, 2003.

826 Stokes, M., Mather, A.E., Belfoul, A., Farik, F.: Active and passive tectonic controls for transverse

827 drainage and river gorge development in a collisional mountain belt (Dades Gorges, High Atlas

828 Mountains, Morocco). *Geomorphology*, 102(1), 2-20,

829 <https://doi.org/10.1016/j.geomorph.2007.06.015>, 2008.

830 Stokes, M., Mather, A.E., Harvey, A.M.: Quantification of river-capture-induced base-level changes
831 and landscape development, Sorbas Basin, SE Spain. *Geol. Soc. London Spec. Publ.*, 191(1),
832 23-35, <https://doi.org/10.1144/GSL.SP.2002.191.01.03>, 2002.

833 Sun, D.H., Bloemendal, J., Rea, D.K., An, Z.S., Vandenberghe, J., Lu, H.Y., Sun, R.X., Liu, T.S.:
834 Bimodal grain-size distribution of Chinese loess, and its palaeoclimatic implications. *Catena*,
835 55(3), 325-340, [https://doi.org/10.1016/S0341-8162\(0300109-7](https://doi.org/10.1016/S0341-8162(0300109-7), 2004.

836 Sun, D.H., Bloemendal, J., Rea, D.K., Vandenberghe, J., Jiang, F.C., An, Z.S., Su, R.X.: Grain-size
837 distribution function of polymodal sediments in hydraulic and aeolian environments, and
838 numerical partitioning of the sedimentary components. *Sediment. Geol.*, 152(3-4), 263-277,
839 [https://doi.org/10.1016/S0037-0738\(0200082-9](https://doi.org/10.1016/S0037-0738(0200082-9), 2002.

840 Sun, J.M., Li, S.H., Muhs, D. R., Li, B.: Loess sedimentation in Tibet: provenance, processes, and
841 link with Quaternary glaciations, *Quat. Sci. Rev.*, 26(17-18), 2265-2280,
842 <https://doi.org/10.1016/j.quascirev.2007.05.003>, 2007.

843 Tan, X.B., Liu, Y.D., Lee, Y.H., Lu, R.Q., Xu, X.W., Suppe, J., Shi, F., Xu, C.: Parallelism between
844 the maximum exhumation belt and the Moho ramp along the eastern Tibetan Plateau margin:
845 Coincidence or consequence?. *Earth Planet. Sci. Lett.*, 507, 73-84,
846 <https://doi.org/10.1016/j.epsl.2018.12.001>, 2019.

847 Tsoar, H., Pye, K.: Dust transport and the question of desert loess formation. *Sedimentology*, 34(1),
848 139-153, <https://doi.org/10.1111/j.1365-3091.1987.tb00566.x>, 1987.

849 Vandenberghe, J.: Grain size of fine-grained windblown sediment: a powerful proxy for process
850 identification. *Earth Sci. Rev.*, 121, 18-30, <https://doi.org/10.1016/j.earscirev.2013.03.001>,
851 2013.

852 Wang, J., Jin, Z.D., Hilton, R.G., Zhang, F., Densmore, A.L., Li, G., West A.J.: Controls on fluvial
853 evacuation of sediment from earthquake-triggered landslides. *Geology*, 43(2), 115-118,
854 <https://doi.org/10.1130/G36157.1>, 2015.

855 Wang, P., Zhang, B., Qiu, W.L., Wang, J.C.: Soft-sediment deformation structures from the Diexi
856 paleo-dammed lakes in the upper reaches of the Minjiang River, east Tibet. *J. Asian Earth Sci.*,
857 40(4), 865-872, <https://doi.org/10.1016/j.jseae.2010.04.006>, 2011.

858 Wang, P., Scherler, D., Liu-Zeng, J., Mey, J., Avouac, J.P., Zhang, Y., Shi, D.: Tectonic control of
859 Yarlung Tsangpo gorge revealed by a buried canyon in southern Tibet. *Science*, 346, 978-981,
860 <https://doi.org/10.1126/science.1259041>, 2014.

861 Wang, W., Godard, V., Liu-Zeng, J., Scherler, D., Xu, C., Zhang, J.Y., Xie, K.J., Bellier, O.,
862 Ansberque, C., Sigoyer, J., Team, A.: Perturbation of fluvial sediment fluxes following the
863 2008 Wenchuan earthquake. *Earth Surf. Process Land.*, 42(15), 2611-2622,
864 <https://doi.org/10.1002/esp.4210>, 2017.

865 Wang, W., Godard, V., Liu-Zeng, J., Zhang, J.Y., Li, Z.G., Xu, S., Yao, W.Q., Yuan, Z.D., Aumaître,
866 G., Bourlès, D.L., Keddadouche, K.: Tectonic controls on surface erosion rates in the Longmen
867 Shan, eastern Tibet. *Tectonics*, 40(3), <https://doi.org/10.1029/2020TC006445>, 2021.

868 Wang, X.G., Li, C.Y., Lu, L.X., Dong, J.B.: Analysis of the late Quaternary activity along the
869 Wenchuan-Maoxian fault-middle of the back- range fault at the Longmen Shan fault zone.
870 *Seism. Geol.*, 39(3), 572-586, <https://doi.org/10.3969/j.issn.0253-4967.2017.03.010>, 2017.

871 Weltje, G.L.: End-member modeling of compositional data: Numerical-statistical algorithms for
872 solving the explicit mixing problem. *Mathemat. Geol.*, 29(4), 503-549,
873 <https://doi.org/10.1007/BF02775085>, 1997.

874 Wei, X.T., Jiang, H.C., Xu, H.Y., Fan, J.W., Shi, W., Guo, Q.Q., Zhang, S.Q.: Response of
875 sedimentary and pollen records to the 1933 Diexi earthquake on the eastern Tibetan Plateau.
876 *Ecol. Indicators*, 129, 107887, <https://doi.org/10.1016/j.ecolind.2021.107887>, 2021.

877 Whipple, K.X.: Bedrock rivers and the geomorphology of active orogens. *Ann. Rev. Earth Planet.*
878 *Sci.*, 32, 151-185, <https://doi.org/10.1146/annurev.earth.32.101802.120356>, 2004.

879 Whittaker, A.C., Attalw, M., Allenn, P.A.: Characterising the origin, nature and fate of sediment
880 exported from catchments perturbed by active tectonics. *Basin Res.*, 22, 809-828,
881 <https://doi.org/10.1111/j.1365-2117.2009.00447.x>, 2010.

882 Whittaker, A. C., Cowie, P.A., Attal, M., Tucker, G. E., Roberts, G.P.: Contrasting transient and
883 steady-state rivers crossing active normal faults: new field observations from the central
884 Apennines, Italy. *Basin Res.*, 19(4), 529-556, <https://doi.org/10.1111/j.1365-2117.2007.00337>,
885 2007.

886 Wu, H.B., Liu, X.M., Lv, B., Ma, M.M., Ji, J.P., Wang, W.Y., Zhang, Y.Y., Hou, J.L.: Aeolian origin

887 of the Twelve Apostles section, in Australia. *Quat. Sci.*, 37(1), 82-96,
888 <https://doi.org/10.11928/j.issn.1001-7410.2017.01.08>, 2017 (in Chinese).

889 Wobus, C., Heimsath, A., Whipple, K. Hodges, K.: Active out-of-sequence thrust faulting in the
890 central Nepalese Himalaya. *Nature*, 434, 1008-1011, <https://doi.org/10.1038/nature03499>,
891 2005.

892 Wobus, C.W., Tucker, G.E., and Anderson, R.S.: Does climate change create distinctive patterns of
893 landscape incision? *J. Geophys. Res.*, 115, F04008, <https://doi.org/10.1029/2009JF001562>,
894 2010.

895 Xu, C., Xu, X.W., Dai, F.C., Xiao, J.Z., Tan, X.B., Yuan, R.M.: Landslides hazard mapping using
896 GIS and weight of evidence model in Qingshui River watershed of 2008 Wenchuan earthquake
897 struck region. *J. Earth Sci.*, 23(1), 97-120, <https://doi.org/10.1007/s12583-012-0236-7>, 2012.

898 Xu, C., Xu, X.W., Yao, X., Dai, F.C.: Three, nearly complete inventories of landslides triggered by
899 the May 12, 2008 Wenchuan Mw 7.9 earthquake of China and their spatial distribution
900 statistical analysis. *Landslides*, 11(3), 441-461, <https://doi.org/10.1007/s10346-013-0404-6>,
901 2014.

902 Xu, H.Y., Jiang, H.C., Liu, K., Zhong, N.: Potential pollen evidence for the 1933 M7.5 Diexi
903 earthquake and implications for post-seismic landscape recovery. *Enviro. Res. Lett.*, 15:094043,
904 <https://doi.org/10.1088/1748-9326/ab9af6>, 2020.

905 Xu, H.Y., Jiang, H.C., Yu, S., Yang, H.L., Chen, J.: OSL and pollen concentrate 14C dating of
906 dammed lake sediments at Maoxian, east Tibet, and implications for two historical earthquakes
907 in AD 638 and 952. *Quat. Inter.*, 371, 290-299, <https://doi.org/10.1016/j.quaint.2014.09.045>,
908 2015.

909 Zhang, F., Jin, Z.D., West, A.J., An, Z.S., Hilton, R.G., Wang, J., Li, G., Densmore, A.L., Yu, J.M.,
910 Qiang, X.K., Sun, Y.B., Li, L.B., Gou, L.F., Xu, Y., Xu, X.W., Liu, X.X., Pan, Y.H., You, C.F.:
911 Monsoonal control on a delayed response of sedimentation to the 2008 Wenchuan earthquake.
912 *Sci. Adv.*, 5(6), eaav7110, <https://doi.org/10.1126/sciadv.aav7110>, 2019.

913 Zhang, P.Z., Deng, Q.D., Zhang, M.G., Ma, J., Gan, W.J., Wei, M., Mao, F.Y., Wang, Q.: Active
914 tectonic blocks and strong earthquakes in the continent of China. *Sci. China*, 46, 13-24,
915 <https://doi.org/10.3969/j.issn.1674-7313.2003.z2.002>, 2003.

916 Zhang, P.Z., Zhou, Z.Y., Xu, C.H., Zhang, Q.L.: Geochemistry of Pengguan complex in the
 917 Longmenshan region, western Sichuan Province, SW China: petrogenesis and tectonic
 918 implications. *Geotecton. Metallog.*, 32(1), 105-116, [https://doi.org/10.3969/j.issn.1001-](https://doi.org/10.3969/j.issn.1001-1552.2008.01.014)
 919 [1552.2008.01.014](https://doi.org/10.3969/j.issn.1001-1552.2008.01.014), 2008 (in Chinese).

920 Zhang, S.Q., Jiang, H.C., Fan, J.W., Xu, H.Y., Shi, W., Guo, Q.Q. and Wei, X.T.: Accumulation of
 921 a last deglacial gravel layer at Diexi, eastern Tibetan Plateau and its possible seismic
 922 significance. *Front. Earth Sci.*, 9:797732, <https://doi.org/10.3389/feart.2021.797732>, 2021.

923 Zhang, Y.Q., Yang, N., Meng, H.: Deep-incised valleys along the Minjiang river upstream and their
 924 responses to the uplift of the West Sichuan Plateau, China. *J. Chengdu Univ. Technol.*, 32(4),
 925 331-339, <https://doi.org/10.3969/j.issn.1671-9727.2005.04.001>, 2005 (in Chinese).

926 Zhou R.J., Li, Y., Densmore, A.L., Ellis, M.A., He, Y.L., Wang, F.L., Li, X.G.: Active tectonics of
 927 the eastern margin of the Tibet Plateau. *J. Mineral. Petrol.*, 26(2),40-51,
 928 <https://doi.org/10.3969/j.issn.1001-6872.2006.02.007>, 2006 (in Chinese).

929 Zhou, R.J., Pu, X.H., He, Y.L., Li, X.G., Ge, T.Y.: Recent activity of Minjiang fault zone, uplift of
 930 Minshan Block and their relationship with seismicity of Sichuan. *Seism. Geol.*, 22(3),285-294,
 931 <https://doi.org/CNKI:SUN:DZDZ.0.2000-03-009>, 2000 (in Chinese).

932 Zhou, R.Y., Wen, X.Y., Lu, L., Li, Y.X., Huang, C.M.: Holocene paleosols and paleoclimate for the
 933 arid upper Minjiang River valley in the eastern Tibetan Plateau. *Catena*, 206, 105555,
 934 <https://doi.org/10.1016/j.catena.2021.105555>, 2021.

935 Zhong, N., Jiang, H.C., Li, H.B., Xu, H.Y., Shi, W., Zhang, S.Q., Wei, X.T.: Last Deglacial Soft-
 936 Sediment Deformation at Shawan on the Eastern Tibetan Plateau and Implications for
 937 Deformation Processes and Seismic Magnitudes. *Acta Geol. Sinica*, 93(2), 430-450,
 938 <https://doi.org/10.1111/1755-6724.13773>, 2019.

939 Zhong, N., Song, X.S., Xu, H.Y., Jiang, H.C.: Influence of a tectonically active mountain belt on its
 940 foreland basin: Evidence from detrital zircon dating of bedrocks and sediments from the eastern
 941 Tibetan Plateau and Sichuan Basin, SW China. *J. Asian Earth Sci.*, 146, 251-264,
 942 <https://doi.org/10.1016/j.jseaes.2017.05.035>, 2017.

943 Zondervan, J., Stokes, M., Boulton, S., Telfer, M., Mather, A.: Rock strength and structural controls
 944 on fluvial erodibility: Implications for drainage divide mobility in a collisional mountain belt.

945 Earth Planet. Sci. Lett., 538, 116221, <https://doi.org/10.1016/j.epsl.2020.116221>, 2020.